Electrochimica Acta 208 (2016) 1–9

Contents lists available at ScienceDirect

Electrochimica Acta

journal homepage: www.elsevier.com/locate/electacta

Nitrogen and gold nanoparticles co-doped carbon nanofiber hierarchical structures for efficient hydrogen evolution reactions

Ming Zhang*, ShuaiShuai Wang, Tao Li, JiaDong Chen, Han Zhu, MingLiang Du

College of Materials and Textiles, Zhejiang Sci-Tech University, Hangzhou 310018, PR China

ARTICLE INFO

Article history:
Received 15 February 2016
Received in revised form 19 April 2016
Accepted 19 April 2016
Available online 7 May 2016

Keywords:
Gold nanoparticles
Nitrogen-doped carbon nanostructures
Carbon nanofibers
Hydrogen evolution reaction

ABSTRACT

A novel hierarchical structure was fabricated by integrating gold nanoparticles (AuNPs) on nitrogen-doped carbon nanorods encapsulating carbon nanofibers (AuNPs@NCNRs/CNFs), and the composite was demonstrated as an electrocatalyst for the hydrogen evolution reaction (HER). First, polyaniline nanorods (PNRs) were grown on the surfaces of the CNFs, and the PNR/CNF hybrids were then decorated with small, well-dispersed and size-controlled AuNPs. The morphology, structure and chemical states of the AuNPs@NCNRs/CNFs hybrids were characterized by field emission scanning electron microscope (FE-SEM), transmission electron microscope (TEM), X-ray diffraction (XRD) and X-ray photoelectron spectroscopy (XPS). The AuNPs@NCNRs/CNFs can be used directly as an electrode and exhibit good HER activity with a relatively low onset potential of 126 mV, a Tafel slope of 93 mV dec^{-1} and remarkable durability in 0.5 M H_2SO_4. The enhancement of the HER activity could be attributed to the synergetic effect between the nitrogen-doped carbon fibers and the AuNPs.

1. Introduction

Developing new electrocatalysts to produce renewable and clean energy from abundant and easily accessible resources is among the most challenging and demanding tasks for today's scientists and engineers. Due to its high calorific value and the fact that it is clean, pollution-free, environmentally friendly, and produces low-carbon energy, hydrogen is considered one of the most promising green energy sources of the 21st century [1,2]. Thus, the ability to effectively produce hydrogen has become one of the most active research areas [3]. The ability to electrochemically split water into hydrogen and oxygen has been realized for over 200 years. Nonetheless, highly effective, earth-abundant catalysts for the hydrogen evolution reaction (HER) and oxygen evolution reaction (OER) are still in high demand [4]. Thus far, noble metal catalysts, which are comprised of industrial and platinum group metals, have been the most widely used electrocatalytic materials and remain the most efficient catalysts for the HER, capable of driving significant currents close to their thermodynamic potentials.

To enhance the electrocatalytic activity of carbon-based materials, many heteroatom-doped carbon-based materials have been extensively studied. For example, Nitrogen and phosphorus dual-doped graphene has been discovered to be an efficient HER catalyst, which showed significantly improved electrochemical performance compared with single doped counterparts [5]. Cobalt and nitrogen co-doped nanocarbons were also studied and found that it exhibited a remarkable electrocatalytic activity toward HER and stability at all pH value (pH 0–14) [6,7]. Typically, rich reserves of 3d transition metals (TMs) on the earth such as Fe, Co and Ni have been proven to be promising catalytic materials for HER in alkaline conditions [8–12]. However, 3d TMs are unstable in acidic conditions, thus limiting their application [13]. Due to the good catalytic activity and stability, AuNPs have proven to be a good catalyst for HER [14,15].

For a long time, the applicability of non-metallic catalysts to water splitting was overlooked. Zou et al. have summarized some noble metal-free catalysts for HER and indicate that the non-precious-metal catalysts exhibit promising and appealing applications in water splitting [16]. In recent studies, nitrogen-containing carbon materials have received increasing attention because nitrogen incorporation enhances the electron-donor or basic capacities of the carbon material, thereby enhancing its electrocatalytic activity [17]. According to previous reports, the electrocatalytic performance of the nitrogen-doped carbon materials based on different nitrogen sources is obviously diverse [18]. The enhanced catalytic activity of these materials can be associated with lone electron pairs of the pyridinic Ns and the presence of

* Corresponding author. Tel: 86 0571 86843255.
E-mail address: zhangming@zstu.edu.cn (M. Zhang).

http://dx.doi.org/10.1016/j.electacta.2016.04.104
0013-4686/

more electrons in the delocalized π-orbitals of the carbon framework (due to the higher number of electrons from the nitrogen atoms*) [19]. Nitrogen-doped carbon materials are widely used in the oxygen reduced reaction (ORR) but rarely for the hydrogen evolution reaction (HER). [20–22] We propose modifying nitrogen-doped carbon materials with a metal to improve the overall current density of the HER. Due to the advantages of fine particle and size controllability, AuNPs have been widely used in sensors [23], electrochemical biorecognition-signaling systems [24], Fenton reactions by light, [25] the ORR [26], etc., but rarely for the HER.

Herein, we attempted to design a new structure by integrating AuNPs on nitrogen-doped carbon nanorods encapsulating carbon nanofibers (AuNPs@NCNRs/CNFs) as the electrode material for the HER. In the present investigation, polyaniline nanorods (PNRs) were first grown on the surfaces of CNFs, and the PNR/CNF hybrid were then decorated with small, well-dispersed and size-controlled AuNPs. The AuNPs@NCNRs/CNFs were prepared through chemical complexation followed by a carbonization process. The associated morphology, microstructure and electrocatalytic performance were further investigated and are discussed below.

2. Experimental

2.1. Materials

Polyacrylonitrile (PAN), perchloric acid ($HClO_4$), aniline, dimethyl formamide (DMF), and thioglycolic acid (TA) were all purchased from Aladdin Chemistry Co., Ltd. Ammonium persulfate (APS) and chloroauric acid ($HAuCl{\cdot}4H_2O$, 99.9%) were purchased from Shanghai Civi Chemical Technology Co., Ltd. All of the reagents were used without further purification. Deionized water (DIW, 18.2 MΩ) was used for all solution preparations.

2.2. Preparation of PAN-based carbon nanofibers (CNFs)

Typically, 5 g of PAN powder was dissolved in 45 ml DMF under magnetic stirring at 65 °C and then electrospun into PAN nanofibers. The voltage, distance and fluid flow rate were 15 kV, 20 cm and 0.6 ml h^{-1}, respectively. Subsequently, the CNFs were prepared by pre-oxidation at 280 °C in air and subsequent carbonization of the PAN nanofibers under Ar atmosphere at 1000 °C. The heating rate was 5 °C min^{-1} in both cases.

2.3. Fabrication of NCNRs/CNFs

The PANI nanorod (PNR)/CNF nanostructures were first synthesized through an *in situ* reaction between the CNFs and an aniline solution under nitrogen protection. The typical steps of this process are as follows: 50 mg CNFs were added to a 0.01 M aniline monomer solution under mild stirring, after which 4 ml of perchloric acid was added to the unreacted suspension. After stirring for 20 min, 1 ml of anhydrous ethanol was dropped slowly into the mixture. Next, 40 ml of 0.04 M APS solution was added to the suspension drop by drop, and polymerization was accomplished via an ice bath. When the solution became blackish green, the mixture was stirred mildly for another 5–6 h. Finally, the resulting PNRs/CNFs were washed with deionized water and anhydrous ethanol three times and dried for 36 h at 30 °C. The nitrogen-doped carbon nanorods (NCNRs)/CNFs were obtained by calcining the PNRs/CNFs under the protection of Ar gas.

2.4. Fabrication of AuNPs@NCNRs/CNFs

First, 200 mg of PNRs/CNFs was added to 1 M ammonia for 30 min and then washed with deionized water and ethanol several times. The resulting samples were mixed with 0.6 g TA solution under mild stirring for 1 h. The mixture was then re-dispersed in

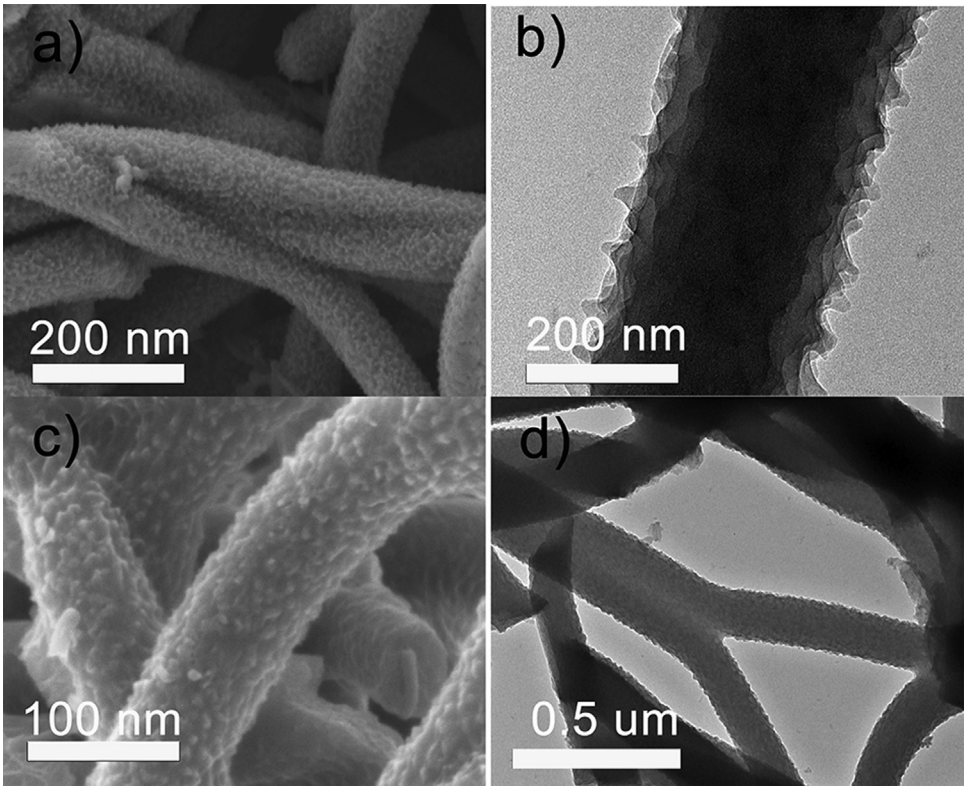

Fig. 1. FE-SEM and TEM images of (a, b) PNRs/CNFs, and (c, d) NCNRs/CNFs.

deionized water, and 8 ml of a 10 M $HAuCl_4$ solution was slowly added to the mixture drop by drop. The reaction was slowly stirred for 24 h at room temperature, and the obtained product was repeatedly washed with deionized water and ethanol. Then, the obtained products were calcined at 800 °C for 2 h under an Ar atmosphere. In this process, $HAuCl_4$ was reduced to metallic AuNPs, which grew on the surfaces of the NCNRs/CNFs.

2.5. Electrochemical characterizations

The catalyst inks were prepared by dispersing 3 mg of each catalyst into 1 ml isopropanol/water solution (75/25 volumetric ratio), and 25 μl Nafion solution (5 wt%, Alfa Aesar) was added to the ink as a proton-conducting binder to ensure suitable adhesion onto the electrode. The catalyst ink was ultrasonicated for 30 min to generate a homogeneous ink. Then, 5 μl of each catalyst ink was transferred onto a glassy carbon electrode (Φ 3 mm) that was previously buff-polished using an alumina suspension. The catalyst loading on the working electrode was 212 μg cm^{-2} after drying at 60 °C for 30 min.

Electrochemical experiments were performed with an electrochemical workstation (CHI660E) equipped with a typical three-electrode configuration accompanied by gas flow systems at 25 °C. Platinum mesh was used as the counter electrode. A saturated calomel electrode (SCE) ($Hg/HgCl_2$ in saturated KCl), which has been calibrated by standard hydrogen electrode, served as the reference electrode with respect to the 0.5 M H_2SO_4 electrolyte. A glassy carbon electrode coated with catalytic ink was directly utilized as the working electrode. The electrolyte was degassed by bubbling with Ar for 30 min prior to the start of each experiment.

2.6. Characterizations

Field emission scanning electron microscopy (FE-SEM) images were characterized using JSM-6700F FE-SEM instrumentation (JEOL, Japan) and an acceleration voltage of 3 kV. Transmission electron microscopy (TEM) images were taken using a JSM-2100 transmission electron microscope (JEOL, Japan) at an acceleration voltage of 200 kV. High-angle annular dark-field scanning transmission electron microscopy (HAADF-STEM) images, STEM mapping, and line-scan energy dispersive X-ray spectroscopy (EDX) images were recorded using STEM instrumentation (Tecnai G2 F30S-Twin, Philips-FEI) and an acceleration voltage of 300 kV. X-ray diffraction (XRD) patterns were analyzed using a Bruker AXS D8 DISCOVER X-ray diffractometer with Cu K_α radiation (λ = 1.5406 Å) at a scanning rate of 0.02 2θ s^{-1} in the 2θ range of 10–80°. X-ray photoelectron spectra of the products were recorded using an X-ray photoelectron spectrometer (Kratos Axis Ultra DLD) with an Al (mono) K_α source (1486.6 eV). The Al K_α source was operated at 15 kV and 10 mA.

3. Results and discussion

The morphology of pure CNFs is shown in Fig. S1a and S1b, and the CNFs exhibit smooth surfaces and diameters ranging from 160 to 280 nm. After the growth of PANI, nanorod-like PANI aligns vertically on the surfaces of the CNFs (Fig. 1a and 1b), leading to the formation of rough surfaces. Subsequently, after carbonization of the as-obtained PNRs/CNFs, the NCNRs/CNFs nanostructures were fabricated. As shown in Fig. 1c and 1d, the NCNR arrays grow throughout the CNF surfaces, and all CNFs are encapsulated with NCNR arrays. Associated STEM-EDS mapping images (Fig. 2) suggest that carbon and nitrogen are uniformly distributed throughout the CNFs, indicating that the CNFs are completely surrounded by the grown NCNRs. The EDS line-scan spectra confirm the uniform distribution of carbon and nitrogen throughout the CNFs. This unique structure and nitrogen-doping will be advantageous for enhancing the electrocatalytic performance for the HER.

XPS was used to further investigate the surface compositions and chemical states of NCNRs/CNFs (Fig. 3a, 3b). The XPS survey spectrum of NCNRs/CNFs exhibits three peaks corresponding to C 1s, N 1s and O 1s (Fig. S2). As shown in Fig. 3a, the C 1s spectrum of NCNRs/CNFs can be fitted into three main peaks with binding energies of 284.6, 285.2 and 286.2 eV, which are attributed to C (sp^2), C (sp^3) and C—OH/C—N, respectively. In Fig. 3b, the N1s spectrum can be de-convoluted into three peaks, pyridinic N (398.2 eV), pyrrolic or pyridonic N (400.3 eV) and quaternary N (401.0 eV) and the percentage of these three types of nitrogen atoms are 36.10%, 35.22%, and 28.57%, respectively [27]. The presence of quaternary N within the graphitic structure is expected to enhance the conductivity of carbon materials. The XPS results show that the nitrogen content is as high as 8.02%. The accessible pyridinic N, pyrrolic and pyridonic N should provide chemically active sites for the HER and can strongly enhance the associated electrocatalytic activity for the HER [28–30].

The HER performance of the PNRs/CNFs and NCNRs/CNFs is shown in Fig. 4 The catalysts were coated on a glassy carbon electrode, and the tests were conducted with a typical three-electrode cell system in a 0.5 M H_2SO_4 electrolyte. Fig. 4a shows the linear sweep voltammogram (LSV) of the samples, and the pure CNFs basically exhibit no HER performance. Own to the onset overpotential is actually a poorly-defined term thus we define onset overpotential as the potential when the current density is 0.5 mA cm^{-2} [16]. Compared with PNRs/CNFs, NCNRs/CNFs exhibit substantially improved electrocatalytic activity with lower onset

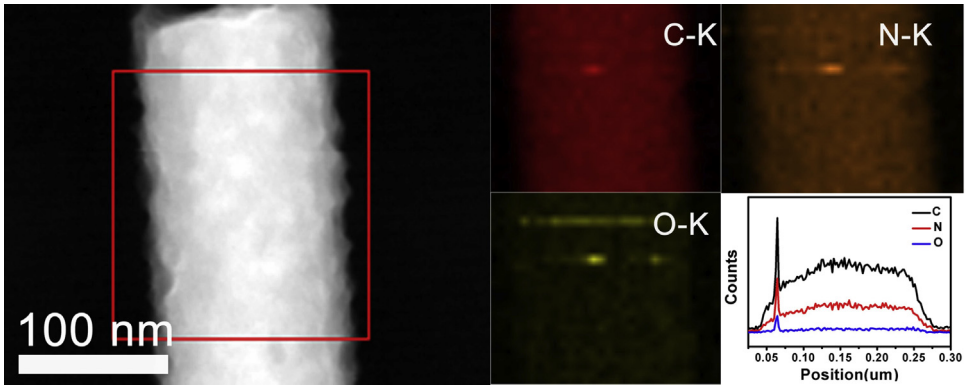

Fig. 2. HAADF-STEM and STEM-EDS mapping images of NCNRs/CNFs.

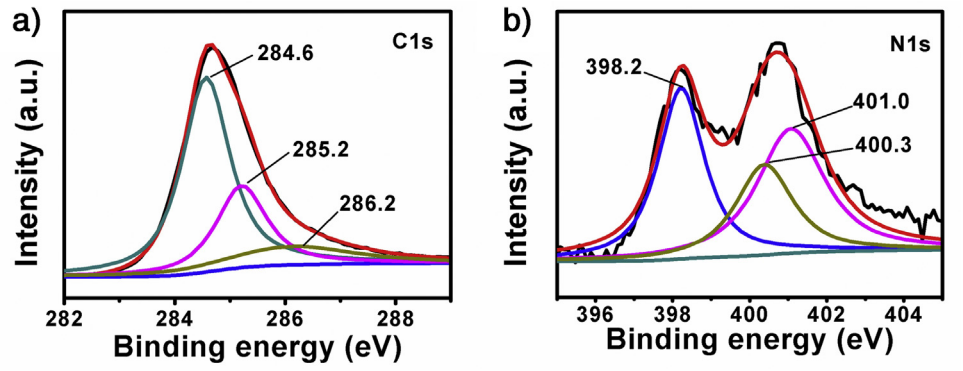

Fig. 3. (a) XPS survey spectra of NCNRs/CNFs, (b) C1s and (c) N1s XPS spectra of NCNRs/CNFs. (d) XRD patterns of CNFs, PNRs/CNFs and NCNRs/CNFs.

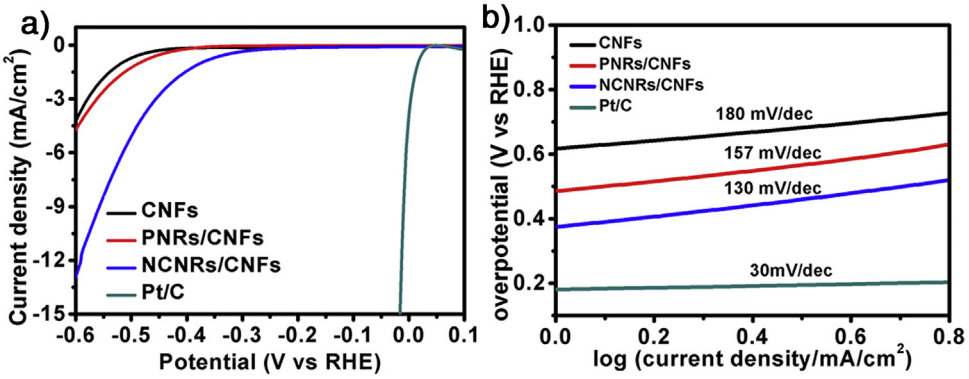

Fig. 4. (a) Polarization performance curves of CNFs, PNRs/CNFs and NCNRs/CNFs recorded in 0.5 M H_2SO_4 at a scan rate of 2 mV s^{-1}. (b) The corresponding Tafel plots of the various electrodes.

overpotentials of approximately 326 mV, while the onset potential of PNRs/CNFs are approximately 446 mV (Fig. 4a). The Tafel slope was determined by fitting the linear portions of the Tafel line. As shown in Fig. 4b, the CNFs show a Tafel slope of 180 mV dec^{-1}, and the NCNRs/CNFs exhibit a Tafel slope of 130 mV dec^{-1}, much lower than that of the PNRs/CNFs (157 mV dec^{-1}). The commercial Pt/C control electrode exhibits the lowest slope, which is 30 mV dec^{-1}. These results show that N-doping can promote the electrocatalytic activities, leading to a relatively lower onset potential.

Durability is another important criterion for evaluating electrocatalytic performance and guaranteeing sustainable hydrogen production. To study the long-term stability of the NCNRs/CNFs, we conducted continuous cyclic voltammetry from −0.8 to 0.2 V vs RHE at 50 mV s^{-1} in 0.5 M H_2SO_4. As shown in Fig. 5, the results suggest that after 1000 cycles, the catalyst still exhibits high cycling stability with only a slight loss in the cathodic current, suggesting the good stability of NCNRs/CNFs electrode.

We can conclude from the above results that nitrogen-doped carbon material can be used as a catalytic material for hydrogen evolution, but the onset potential is still relatively high, the current density is low, and the Tafel slope is too high. Therefore, introducing other catalysts is necessary to enhance the HER performance. Combining good chemical stability with relatively high HER activity [31], AuNPs were employed to further improve the catalytic performance of the NCNRs/CNFs electrode.

The morphology of the AuNPs@NCNRs/CNFs is shown in Fig. 6. The size of the AuNPs on the NCNRs/CNFs can be adjusted by changing the concentration of the $HAuCl_4$. Therefore, apart from adding 8 ml of 10 M $HAuCl_4$ solution, we also added 16 ml and 24 ml of the $HAuCl_4$ solution to prepare different AuNPs@NCNRs/CNFs products, and the three samples were labeled AuNPs@NCNRs/CNFs-8, AuNPs@NCNRs/CNFs-16, and AuNPs@NCNRs/CNFs-24. In addition, we also prepared Au nanoparticles doped carbon nanofiber (AuNPs/CNFs) as control (Fig. S3). For the AuNPs@NCNRs/CNFs-8, uniform and small AuNPs are well dispersed on the surfaces of NCNRs/CNFs, the AuNPs are the most sparsely distributed, and the size of the AuNPs is the smallest among the samples (Fig. 6a–f). With the increasing amount of $HAuCl_4$, the particles become larger and their distribution becomes denser. All the AuNPs are well dispersed throughout the NCNRs/CNFs, and there are almost no aggregated AuNPs. The high-resolution TEM (HR-TEM) image (Fig. 6g) clearly displays typical AuNPs grown on the NCNRs/CNFs. As shown in Fig. 6g, the interfringe distances of 0.14 nm and 0.23 nm correspond to the (220)

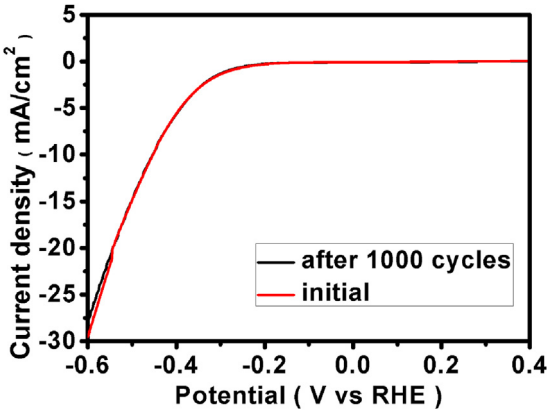

Fig. 5. The durability test after 1000 cycles of the NCNRs/CNFs.

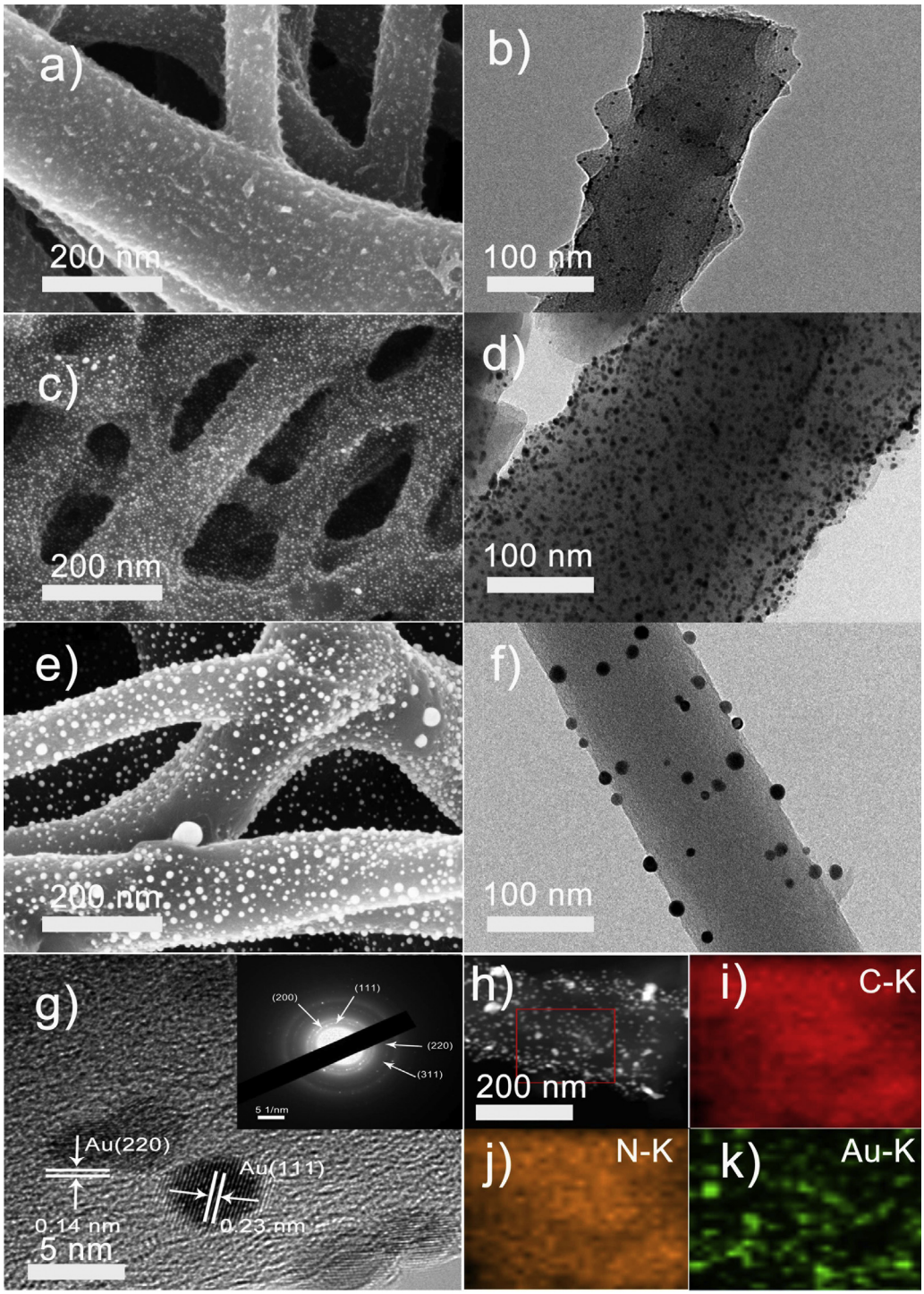

Fig. 6. FE-SEM and TEM images of the AuNPs@NCNRs/CNFs-8 (a), (b); AuNPs@NCNRs/CNFs-16 (c), (d); and AuNPs@NCNRs/CNFs-24 (e), (f); HR-TEM images of the AuNPs@NCNRs/CNFs-2 (g), inset of (g) is the SAED pattern. (h) STEM, (i–k) STEM-EDS element mapping images of the AuNPs@NCNRs/CNFs.

and (111) planes of the AuNPs. The selected area electron diffraction (SAED) pattern of the AuNPs@NCNRs/CNFs (inset of Fig. 6g) reveals the polycrystalline diffraction rings indexed to the (200), (111), (220), and (311) planes of fcc gold [23], indicating the polycrystallinity of the AuNPs. To further explore the morphology of the AuNPs@NCNRs/CNFs-16, the HAAD-STEM image and STEM-EDS mapping are shown in Fig. 6h–k. The carbon and nitrogen can be clearly observed throughout the NCNRs/CNFs, indicating the successful synthesis of N-doped carbon. Fig. 6k exhibits the Au element signals, and the green spot are well matched with the morphologies of AuNPs in the mapping area (Fig. 6h), demonstrating the formation of AuNPs on the surfaces of NCNRs/CNFs.

The as-obtained samples were characterized by XPS to reveal their chemical composition and states. The overall XPS survey spectra of AuNPs@NCNRs/CNFs demonstrates the existence of carbon, nitrogen and gold in the hybrid (Fig. S4). As shown in Fig. 7a–c, for the Au 4f spectra (Fig. 7a), there are two significant peaks located at 83.3 eV and 87.0 eV, which are in good agreement with the binding energies of Au $4f_{7/2}$ and Au $4f_{5/2}$ [31–33], respectively. The C 1s spectrum of the AuNPs@NCNRs/CNFs-16 is

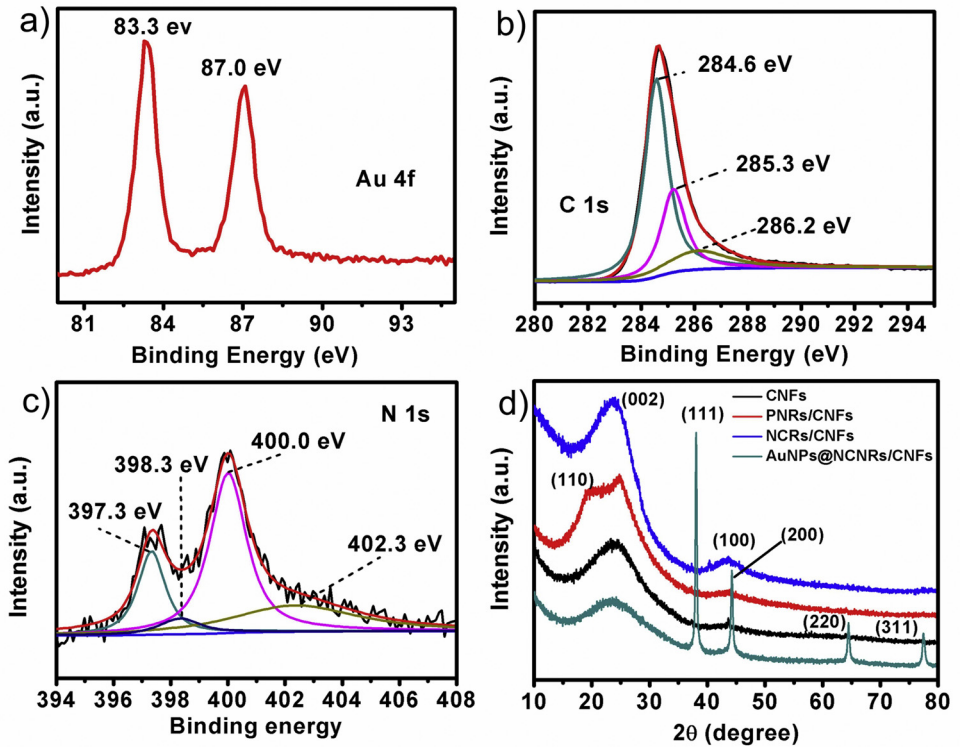

Fig. 7. XPS spectra (a) Au 4f, (b) C 1s and (c) N 1s of the AuNPs@NCNRs/CNFs; (d) XRD spectra of the AuNPs@NCNRs/CNFs, NCNRs/CNFs, PNRs/CNFs and CNFs.

similar to the C 1s spectrum of NCNRs/CNFs, and there are mainly three carbon species present in the samples: C (sp^2) (284.6 eV), C (sp^3) (285.2 eV) and C—OH/C—N (286.2 eV). The high resolution N1s spectra of AuNPs@NCNRs/CNFs-16 can be deconvoluted into four different peaks at binding energy of 397.3 eV, 398.3 eV, 400.0 eV and 402.4 eV, corresponding to pyridinic-N, pyrrolic-N, graphitic-N, and pyridinic-N-oxide [34,35], respectively. In addition, these peaks can be ascribed to the sp^2-hybridized nitrogen involved in triazine rings (C—N=C), the tertiary nitrogen N-$(C)_3$ groups, the free amino groups (C-N-C), and π-excitations, respectively. The percentages of the four types of nitrogen atoms are 18.07%, 15.20%, 47.43%, and 19.30%, respectively.

The XRD pattern of the AuNPs@NCNR/CNF hybrids shows four sharp peaks located at 38.1°, 44.1°, 64.6°, and 77.4°, and they can be indexed to the (111), (200), (220), and (311) planes of fcc gold (JCPDS: 65-2870), respectively, [36,37] which is in good agreement with the HR-TEM image and the SAED pattern (Fig. 6g). These results further verify that the AuNPs@NCNRs/CNFs were successfully prepared. The CNFs exhibit a sharp peak at 24.8° and a small broad peak at 43.8°, corresponding to the (002) and (100) reflections of the pure graphitic lattice of CNFs (JCPDS, No. 75-1621). The PNRs/CNFs not only show the characteristic peaks of CNFs but also exhibit a small characteristic PANI peak at approximately 20°, corresponding to the (110) plane and indicating the successful growth of PANI on the surface of the CNFs [33]. After the carbonization, the peaks of the (002) and (100) planes of NCNRs/CNFs become sharp, and the (110) plane of PANI disappears, suggesting the formation of N-doped carbon nanostructures and increases in the degrees of crystallization and graphitization [38]. However, the (002) peak shifted from $2\theta = 24.8°$ to $2\theta = 23.6°$, which may be related to changes in the structures or valence of the carbon in the hybrid films after nitrogen doping [39,40].

The HER performance of the AuNPs@NCNRs/CNFs with different sizes of AuNPs was measured in an Ar-saturated 0.5 M H_2SO_4 solution using a conventional three-electrode system. The AuNPs@NCNRs/CNF-modified GCE (Φ 3 mm) was used as the working electrode, a platinum mesh was used as the counter electrode, and a saturated calomel electrode (SCE) ($Hg/HgCl_2$ in saturated KCl), which has been calibrated by standard hydrogen electrode, served as the reference electrode. Fig. 8 (a) shows the LSV of the different samples. Compared with CNFs, PNRs/CNFs and NCNRs/CNFs, the AuNPs@NCNRs/CNFs exhibit much lower onset potentials and higher current densities. The onset overpotentials of AuNPs@NCNRs/CNFs-8, AuNPs@NCNRs/CNFs-16, and AuNPs@NCNRs/CNFs-24 are 190 mV, 126 mV and 179 mV, respectively. For the AuNPs@NCNRs/CNFs-8 electrode, deliver a current density of 10 mA cm^{-2} requires approximately 386 mV, and the AuNPs@NCNRs/CNFs-24 require approximately 322 mV to deliver a current density of 10 mA cm^{-2}. The AuNPs@NCNRs/CNFs-16 exhibit the lowest onset potential of approximately 126 mV, upon which the cathodic current density increases rapidly at more negative potentials, and this electrode material requires 288 mV to deliver a current density of 10 mA cm^{-2} (see Table 1), suggesting superior HER activity. The electrocatalytic property of AuNPs/CNFs is poorer than AuNPs@NCNR/CNFs. The onset overpotential of AuNPs/CNFs is 226 mV and it requires 425 mV to deliver a current density of 10 mA cm^{-2}, respectively. The Pt/C electrode shows extraordinary HER activity with an onset potential of approximately 0 V. Meanwhile, the combination of the AuNPs with NCNRs/CNFs indeed improves the HER activity, which is close to that of Pt/C catalysts.

As shown in Fig. 8b, the Tafel slopes of the AuNPs@NCNRs/CNFs-8, AuNPs@NCNRs/CNFs-24 and AuNPs@NCNRs/CNFs-16 are 110 mV dec^{-1}, 102 mV dec^{-1}, 93 mV dec^{-1}, respectively, which are much lower than those of the CNFs (180 mV dec^{-1}), PNRs/CNFs (157 mV dec^{-1}), NCNRs/CNFs (130 mV dec^{-1}) and AuNPs/CNFs (121 mV dec^{-1}). The lower Tafel slopes mean faster kinetics for the HER [41,42].

Electrochemical impedance spectroscopy (EIS) measurements were conducted to investigate (performed at −0.2 V vs RHE) the electrode kinetic during HER process. [43–45] The representative Nyquist plots of the electrocatalysts were shown in Fig. S5. The

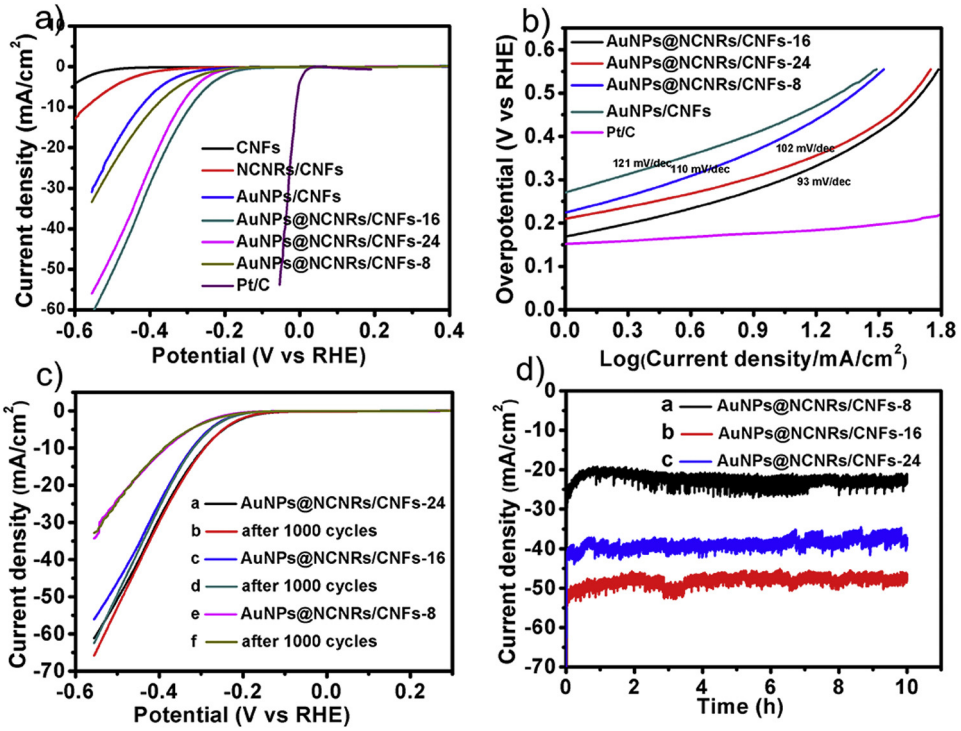

Fig. 8. (a) HER activity of the different catalysts in 0.5 M H_2SO_4 at a scan rate of 2 mV s^{-1}, (b) Tafel plots of the synthesized samples, (c) the durability test of the three AuNPs@NCNRs/CNFs, (d) chronoamperometric response (i–t) of the different AuNPs@NCNRs/CNFs at a constant applied potential of −0.5 V vs RHE.

semicircle in the Nyquist plot of the samples represents the charge transfer process on the interface between electrocatalyst and electrolyte, which are comprised of charge transfer resistance (R_{ct}) and corresponding capacitance. In general, R_{ct} value varies inversely to the electrocatalytic activity. Fig. S5 shows a decreased charge-transfer resistance (R_{ct}) for AuNPs@NCNRs/CNFs-16 relative to AuNPs@NCNRs/CNFs-24 and AuNPs@NCNRs/CNFs-8, indicating the smaller charge transfer resistance of AuNPs@NCNRs/CNFs-16, and such a low R_{ct} indicating its high electrocatalytic activity for HER. The calculated TOF values of the AuNPs@NCNRs/CNFs-8, AuNPs@NCNRs/CNFs-16 and AuNPs@NCNRs/CNFs-24 are 0.023 s^{-1}, 0.049 s^{-1} and 0.032 s^{-1}, respectively, which are well consistent with the experimental measured polarization curves (see the details in the Supporting Information).

To study the long-term stability of the AuNPs@NCNRs/CNFs and NCNRs/CNFs, we conducted continuous cyclic voltammetry from −0.8 to 0.2 V vs RHE at 50 mV s^{-1} in 0.5 M H_2SO_4. The results show that after 1000 cycles, the catalysts exhibit high cycling stability with only a slight loss in the cathodic current, suggesting that the AuNPs@NCNRs/CNFs and NCNRs/CNFs electrodes exhibit good stability (Fig. 8c). The AuNPs@NCNRs/CNFs mat were used directly as an electrode, and the amperometric i-t curves at −0.5 V vs RHE were performed continuously for 10 h using AuNPs@NCNRs/CNFs-8, AuNPs@NCNRs/CNFs-16 and AuNPs@NCNRs/CNFs-24 mat as the working electrodes. As show in Fig. 8d, the current density of these electrodes remained stable for 10 h, and the slight decrease in current density could be ascribed to the continuously released bubbles generated on the surface of the electrodes. The morphologies of the AuNPs@NCNRs/CNFs-8, AuNPs@NCNRs/CNFs-16 and AuNPs@NCNRs/CNFs-24 after electrocatalysis were characterized with FE-SEM (Fig. S6) and found that there is no significant change, furthermore indicating the good stability of the catalysts. This excellent durability shows promise for practical long-term applications of the catalysts. In addition, to ensure the reproducibility of the results, we conducted repeated experiments of the electrochemical measurements and the results indicate that the synthesized materials exhibit good repeatability (see Table 4 in the Supporting Information).

The Pt residues during the electrocatalytic measurements may significantly affect the electrocatalytic parameters. Consequently, to rule out the effect of possible Pt residue in the electrolyte, we performed the electrochemical measurements of AuNPs@NCNR/CNFs using Pt-mesh and carbon rod as counter electrode, respectively. The onset overpotentials of AuNPs@NCNRs/CNFs-8, AuNPs@NCNRs/CNFs-16, and AuNPs@NCNRs/CNFs-24 using carbon rod as counter electrode are 197 mV, 159 mV and 183 mV, respectively (Fig. S7). They are very close to those obtained using Pt-mesh as counter electrode, indicating that there is nearly no Pt residues influencing the electrochemical measurement.

The HER performance of AuNP-decorated NCNRs/CNFs is better than the bare PNRs/CNFs and NCNRs/CNFs due to the strong synergetic effects between AuNPs and the N-doped carbon nanofiber. The introduced AuNPs enhance the electron density and reduce the free energy of the hydrogen atoms and the potentials for hydrogen generation [4].

Table 1
Summary of the HER electrocatalytic activity the synthesized catalysts.

catalyst	b (mV dec^{-1})	η(mV)	η_{10} (mV)
AuNPs@NCNRs/CNFs-8	110	190	386
AuNPs@NCNRs/CNFs-16	93	126	288
AuNPs@NCNRs/CNFs-24	102	179	322

4. Conclusions

In the present investigation, a novel hierarchical structure has been demonstrated by integrating AuNPs on nitrogen-doped carbon nanorods/carbon nanofibers, serving as electrocatalyst for the HER. The PNRs were first grown on the surfaces of CNFs, and

the PNR/CNF hybrids were then decorated with small, well-dispersed and size-controlled AuNPs. The morphologies, nanostructures and chemical states were investigated by SEM, TEM, XRD and XPS. Electrochemical investigations demonstrate that the AuNPs@PNRs/CNFs can be used directly as electrodes and exhibit good HER activity with relatively low onset potentials, Tafel slopes and remarkable durability in 0.5 M H_2SO_4. The HER performance of AuNP-decorated NCNRs/CNFs is much better than the PNRs/CNFs and NCNRs/CNFs due to the strong synergetic effects between AuNPs and N-doped carbon nanofibers. The introduction of AuNPs enhances the electron density and reduces both the free energy of the hydrogen atoms and the potentials for hydrogen generation.

Acknowledgements

This study was supported by the National Natural Science Foundation of China (NSFC) (Grant no. 51573166), the Natural Science Foundation of Zhejiang Province (Grant No. LQ16E020005), Science Foundation of Zhejiang Sci-Tech University (Grant number: 13012116-Y) and the Young Researchers Foundation of Key Laboratory of Advanced Textile Materials and Manufacturing Technology, Ministry of Education, Zhejiang Sci-Tech University (2014QN02), the Foundation of Beijing National Laboratory for Molecular Sciences (BNLMS), Program for Innovative Research Team of Zhejiang Sci-Tech University and the 521 Talent Project of Zhejiang Sci-Tech University.

Appendix A. Supplementary data

Supplementary data associated with this article can be found, in the online version, at http://dx.doi.org/10.1016/j.electacta.2016.04.104.

References

[1] S. Chu, A. Majumdar, Opportunities and challenges for a sustainable energy future, Nature 488 (2012) 294–303.
[2] G. Xie, K. Zhang, B. Guo, Q. Liu, L. Fang, J.R. Gong, Graphene-based materials for hydrogen generation from light-driven water splitting, Adv. Mater. 25 (2013) 3820–3839.
[3] Q. Gong, L. Cheng, C. Liu, M. Zhang, Q. Feng, H. Ye, M. Zeng, L. Xie, Z. Liu, Y. Li, Ultrathin MoS2(1−x)Se2x alloy nanoflakes for electrocatalytic hydrogen evolution reaction, ACS Catal. 5 (2015) 2213–2219.
[4] H. Zhu, J. Zhang, R. Yanzhang, M. Du, Q. Wang, G. Gao, J. Wu, G. Wu, M. Zhang, B. Liu, J. Yao, X. Zhang, When cubic cobalt sulfide meets layered molybdenum disulfide: a core-shell system toward synergetic electrocatalytic water splitting, Adv. Mater. 27 (2015) 4752–4759.
[5] Y. Zheng, Y. Jiao, L.H. Li, T. Xing, Y. Chen, M. Jaroniec, S.Z. Qiao, Taward design of synergistically active carbon-based catalysts for electrocatalytic hydrogen evolution, ACS nano 8 (2014) 5290–5296.
[6] S. Gao, G.D. Li, Y.P. Liu, H. Chen, L.L. Feng, Y. Wang, M. Yang, D.J. Wang, S. Wang, X. Zou, Electrocatalytic H_2 production from seawater over Co, N-codoped nanocarbons, Nanoscale 7 (2015) 2306–2316.
[7] X. Zou, X. Huang, A. Goswami, R. Silva, B.R. Sathe, E. Mikmekova, T. Asefa, Cobalt-embedded nitrogen-rich carbon nanotubes efficiently catalyze hydrogen evolution reaction at all pH values, Angwe. Chem. Int. Ed. 53 (2014) 4372–4376.
[8] J. Deng, P. Ren, D. Deng, L. Yu, F. Yang, X. Bao, Highly active and durable non-precious-matel catalysts encapsulated in carbon nanotubes for hydrogen evolution reaction, Energy Environ. Sci. 7 (2014) 1919–1923.
[9] A. Doner, I. Karci, G. Kardas, Effect of Co-felt supported Ni, Co, and NiCo catalysts to produce hydrogen, Int. J. Hydrogen Energy 37 (2012) 9470–9476.
[10] A. Doner, R. Solmaz, G. Kardas, Enhancement of hydrogen evolution at cobalt-zine deposited graphite electrode in alkaline solution, Int. J. Hydrogen Energy 36 (2011) 7391–7397.
[11] V.V. Kuznetsov, A.A. Kalinkina, T.V. Pshenichkina, V.V. Balabaev, Electrocatalytic properties of cobalt-molybdenum alloy deposits in the hydrogen evolution reaction, Russ. J. Electrochem. 44 (2008) 1350–1358.
[12] M. Torabi, S.K. Sadrnezhaad, Electrochemical synthesis of flake-like Fe/MWCNTs nanocomposite for hydrogen evolution reaction: effect of the CNTs on dendrite growth of iron and its electrocatalytic activity, Curr. Appl. Phys. 10 (2010) 72–76.
[13] B.S. Sun, F. Jaouen, J.P. Dodelet, Cotrolled growth of Pt nanowires on carbon nanospheres and their enhanced performance as electrocatalysts in PEM fuel cells, Adv. Mater. 20 (2008) 3900–3904.
[14] P. Quaino, E. Santos, Hydrogen evolution reaction on palladium multilayers deposited on Au(111): A theoretical approach, Langmuir 31 (2015) 858–867.
[15] H. Lv, Z. Xi, Z. Chen, S. Guo, Y. Yu, W. Zhu, Q. Li, X. Zhang, M. Pan, G. Lu, S. Mu, S. Sun, A new core/shell NiAu/Au nanoparticle catalyst with Pt-like activity for hydrogen evolution reaction, J. Am. Chen. Soc. 137 (2015) 5859–5862.
[16] X. Zou, Y. Zhang, Noble metal-free hydrogen evolution catalysts for water splitting, Chem. Soc. Rev. 44 (2015) 5148–5180.
[17] X. Duan, Z. Ao, H. Sun, S. Indrawirawan, Y. Wang, J. Kang, F. Liang, Z.H. Zhu, S. Wang, Nitrogen-doped graphene for generation and evolution of reactive radicals by metal-free catalysis, ACS Appl. Mat. Interfaces 7 (2015) 4169–4178.
[18] S. Wang, C. Dai, J. Li, L. Zhao, Z. Ren, Y. Ren, Y. Qiu, J. Yu, The effect of different nitrogen sources on the electrocatalytic properties of nitrogen-doped electrospun carbon nanofibers for the oxygen reduction reaction, Int. J. Hydrogen Energy 40 (2015) 4673–4682.
[19] V. Sahu, S. Grover, B. Tulachan, M. Sharma, G. Srivastava, M. Roy, M. Saxena, N. Sethy, K. Bhargava, D. Philip, H. Kim, G. Singh, S.K. Singh, M. Das, R.K. Sharma, Heavily nitrogen doped, graphene supercapacitor from silk cocoon, Electrochim. Acta 160 (2015) 244–253.
[20] L. Zhang, X. Wang, R. Wang, M. Hong, Structural evolution from metal–organic framework to hybrids of nitrogen-doped porous carbon and carbon nanotubes for enhanced oxygen reduction activity, Chem. Mater. 27 (2015) 7610–7618.
[21] B. Zhang, Z. Wen, S. Ci, S. Mao, J. Chen, Z. He, Synthesizing nitrogen-doped activated carbon and probing its active sites for oxygen reduction reaction in microbial fuel cells, ACS Appl. Mat. Interfaces 6 (2014) 7464–7470.
[22] J.D. Wiggins-Camacho, K.J. Stevenson, Mechanistic Discussion of the Oxygen Reduction Reaction at Nitrogen-Doped Carbon Nanotubes, J. Phys. Chem. C 115 (2011) 20002–20010.
[23] P. Ma, H. Zhu, J. Wei, M. Zhang, Facile fabrication of Au nanoparticles immobilized on polyaniline nanofibers: high sensitive nonenzymatic hydrogen peroxide sensor, Nanosci. Nanotech. Let. 7 (2015) 127–133.
[24] A. Sánchez, P. Díez, P. Martínez-Ruíz, R. Villalonga, J.M. Pingarrón, Janus Au-mesoporous silica nanoparticles as electrochemical biorecognition-signaling system, Electrochem. Commun. 30 (2013) 51–54.
[25] S. Navalon, M. de Miguel, R. Martin, M. Alvaro, H. Garcia, Enhancement of the catalytic activity of supported gold nanoparticles for the Fenton reaction by light, J. Am. Chem. Soc. 133 (2011) 2218–2226.
[26] Y. Lee, A. Loew, S. Sun, Surface-and structure-dependent catalytic activity of Au nanoparticles for oxygen reduction reaction, Chem. Mater. 22 (2010) 755–761.
[27] L. Lai, J.R. Potts, D. Zhan, L. Wang, C.K. Poh, C. Tang, H. Gong, Z. Shen, J. Lin, R.S. Ruoff, Exploration of the active center structure of nitrogen-doped graphene-based catalysts for oxygen reduction reaction, Energ. Environ. Sci. 5 (2012) 7936.
[28] Y. Ito, W. Cong, T. Fujita, Z. Tang, M. Chen, High catalytic activity of nitrogen and sulfur co-doped nanoporous graphene in the hydrogen evolution reaction, Angew. Chem. 54 (2015) 2131–2136.
[29] C. Tang, A. Sun, Y. Xu, Z. Wu, D. Wang, High specific surface area Mo2C nanoparticles as an efficient electrocatalyst for hydrogen evolution, J. Power Sources 296 (2015) 18–22.
[30] X. Liu, W. Zhou, L. Yang, L. Li, Z. Zhang, Y. Ke, S. Chen, Nitrogen and sulfur co-doped porous carbon derived from human hair as highly efficient metal-free electrocatalysts for hydrogen evolution reactions, J. Mater. Chem. A 3 (2015) 8840–8846.
[31] H. Zhu, M. Du, M. Zou, C. Xu, N. Li, Y. Fu, Facile and green synthesis of well-dispersed Au nanoparticles in PAN nanofibers by tea polyphenols, J. Mater. Chem. 22 (2012) 9301.
[32] J. Lu, W. Zhou, L. Wang, J. Jia, Y. Ke, L. Yang, K. Zhou, X. Liu, Z. Tang, L. Li, S. Chen, Core-shell nanocomposites based on gold nanoparticle@zinc-iron-embedded porous carbons derived from metal-organic frameworks as efficient dual catalysts for oxygen reduction and hydrogen evolution reactions, ACS Catal. 6 (2016) 1045–1053.
[33] Q. Lin, L. Li, S. Liang, M. Liu, J. Bi, L. Wu, Efficient synthesis of monolayer carbon nitride 2D nanosheet with tunable concentration and enhanced visible-light photocatalytic activities, Appl. Catal. B: Environ. 163 (2015) 135–142.
[34] P. Zamani, D. Higgins, F. Hassan, G. Jiang, J. Wu, S. Abureden, Z. Chen, Electrospun iron–polyaniline–polyacrylonitrile derived nanofibers as non-precious oxygen reduction reaction catalysts for PEM fuel cells, Electrochim. Acta 139 (2014) 111–116.
[35] R.M. Yadav, J. Wu, R. Kochandra, L. Ma, C.S. Tiwary, L. Ge, G. Ye, R. Vajtai, J. Lou, P. M. Ajayan, Carbon Nitrogen Nanotubes as Efficient Bifunctional Electrocatalysts for Oxygen Reduction and Evolution Reactions, ACS Appl. Mat. Interfaces 7 (2015) 11991–12000.
[36] H. Zhang, F. Huang, S. Xu, Y. Xia, W. Huang, Z. Li, Fabrication of nanoflower-like dendritic Au and polyaniline composite nanosheets at gas/liquid interface for electrocatalytic oxidation and sensing of ascorbic acid, Electrochem. Commun. 30 (2013) 46–50.
[37] N. Cheng, J. Tian, Q. Liu, C. Ge, A.H. Qusti, A.M. Asiri, A.O. Al-Youbi, X. Sun, Au-nanoparticle-loaded graphitic carbon nitride nanosheets: green photocatalytic synthesis and application toward the degradation of organic pollutants, ACS Appl. Mat. Interfaces 5 (2013) 6815–6819.
[38] W. Ju, M. Favaro, C. Durante, L. Perini, S. Agnoli, O. Schneider, U. Stimming, G. Granozzi, Pd Nanoparticles deposited on nitrogen-doped HOPG: New Insights into the Pd-catalyzed Oxygen Reduction Reaction, Electrochim. Acta 141 (2014) 89–101.
[39] W. Zhou, K. Zhou, D. Hou, X. Liu, G. Li, Y. Sang, H. Liu, L. Li, S. Chen, Three-dimensional hierarchical frameworks based on MoS2 nanosheets self-

assembled on graphene oxide for efficient electrocatalytic hydrogen evolution, ACS Appl. Mat. Interfaces 6 (2014) 21534–21540.
[40] Y. Zheng, Y. Jiao, L.H. Li, T. Xing, Y. Chen, M. Jaroniec, S.Z. Qiao, Toward design of synergistically active carbon-based catalysts for electrocatalytic hydrogen evolution, ACS nano 8 (2015) 5290–5296.
[41] J.D. Benck, T.R. Hellstern, J. Kibsgaard, P. Chakthranont, T.F. Jaramillo, Catalyzing the Hydrogen Evolution Reaction (HER) with Molybdenum Sulfide Nanomaterials, ACS Catal. 4 (2014) 3957–3971.
[42] Y. Li, H. Wang, L. Xie, Y. Liang, G. Hong, H. Dai, MoS2 nanoparticles grown on graphene: an advanced catalyst for the hydrogen evolution reaction, J. Am. Chem. Soc. 133 (2011) 7296–7299.
[43] J. Duan, S. Chen, M. Jaroniec, S.Z. Qiao, Porous C3N4 nanolayers@N-graphene films as catalyst electrodes for highly efficient hydrogen evolution, ACS nano 9 (2015) 931–940.
[44] E. Navarro-Flores, Z. Chong, S. Omanovic, Characterization of Ni, NiMo NiW, and NiFe electroactive coatings as electrocatalysts for hydrogen evolution in an acidic medium, J. Mol. Catal. A: Chem. 226 (2005) 179–197.
[45] L. Liao, J. Zhu, X. Bian, L. Zhu, M.D. Scanlon, H.H. Girault, B. Liu, MoS_2 formed on mesoporous graphene as a highly active catalyst for hydrogen evolution, Adv. Funct. Mater. 23 (2013) 5326–5333.